Quaternary Science Reviews 334 (2024) 108710

Contents lists available at ScienceDirect

Quaternary Science Reviews

journal homepage: www.elsevier.com/locate/quascirev

Late Holocene tropical cyclones linked to climatic and solar variability

Yang Wang [a,b,*], Shakura Jahan [a,b], William C. Burnett [a,b], Zhaohua Wu [a], James B. Elsner [c], Guy H. Means [d,b], Jin Liu [a,b,e], Shijun Jiang [f]

[a] Department of Earth, Ocean, and Atmospheric Science, Florida State University, Tallahassee, FL, 32306-4520, USA
[b] National High Magnetic Field Laboratory, Tallahassee, FL, 32310, USA
[c] Department of Geography, Florida State University, Tallahassee, FL, 32306, USA
[d] Florida Geological Survey, Florida Department of Environmental Protection, Tallahassee, FL, 32303, USA
[e] School of Civil and Architecture Engineering, Xi'an Technological University, Xi'an, 710021, PR China
[f] College of Oceanography, Hohai University, Nanjing, 210024, PR China

ARTICLE INFO

Handling editor: P Rioual

Keywords:
Geochemical proxies
Hurricanes
Paleoclimate
Gulf of Mexico
North atlantic
Paleotempestology

ABSTRACT

Response of tropical cyclone (TC) frequency to future climate change has important implications for society but remains poorly understood due to a lack of long-term reliable observational records. Here, we use high-resolution organic geochemical proxies (OGPs) with robust chronological control from two coastal lakes, >150 km apart, to reconstruct past TC activities in the northeastern Gulf of Mexico (GOM). Results show multi-decadal-to-centennial-scale fluctuations in TC frequency over the last 5500 years. We found that TC frequency either exceeded or was comparable to modern observations during a prolonged interval (~1500-720 cal yr BP) that encompasses the Medieval Warm Period. We also found a nearly 90% reduction in TC activity, relative to modern, during an exceptionally quiescent period (650-280 cal yr BP) that overlaps the Little Ice Age. Warmer temperatures in the North Atlantic did not always support increased TC frequency in this region. We show, for the first time, that increased TC activities in the northeastern GOM track increased solar irradiance. High TC frequency is also coupled to periods of increased sea surface temperatures in the northern GOM, enhanced El Niño-Southern Oscillation, and positive phases of the Atlantic Multi-Decadal Oscillation. Our results highlight the importance of natural variability in climate and solar activity in modulating TC frequency.

1. Introduction

Landfalling tropical cyclones represent the costliest natural catastrophes in the US (NCEI, 2021). Although future trends in tropical cyclone (TC) activity are uncertain (Knutson et al., 2020), there appears to be a causal relationship between increasing sea surface temperature (SST) and increasing TC intensity and/or frequency in the North Atlantic Basin (Elsner et al., 2008; Goldenberg et al., 2001; Kossin et al., 2020). As oceans warm, they provide more heat energy to be converted to tropical cyclone wind and thus may result in more favorable conditions for developing stronger storms (Elsner et al., 2008). It has been suggested that Atlantic TC activity is thus likely modulated by the Atlantic Multidecadal Oscillation (AMO), an oscillatory climate mode occurring in North Atlantic sea surface temperature (SST) that varies on time scales of 30–80 years (Delworth and Mann, 2000), with warm AMO phases favoring more TCs (Goldenberg et al., 2001). Instrumental records also suggest that El Niño/Southern Oscillation (ENSO), the dominant coupled atmosphere-ocean mode of interannual climate variability, is a key factor in driving TC activity. In general, the Atlantic Basin has fewer TCs during El Niño years than in La Niña years due to stronger vertical wind shear and an overall greater atmospheric stability in El Niño years with some exceptions (Gray, 1984; Kim et al., 2009; Wang and Lee, 2010). Additionally, the location and strength of the Bermuda High, as indicated by the magnitude and sign of the North Atlantic Oscillation (NAO), has been linked to the local frequency of hurricanes along the US coast and across the western Caribbean (Jagger et al., 2002). However, the feedback between AMO, ENSO, NAO and TC activity modulation, especially on longer-time scales, is not well understood (Schmitt et al., 2020). Modeling studies have yielded inconsistent results in projecting future TC activity (Knutson et al., 2020). Understanding precise connections between TC frequency and climate is challenging due to limitations in the length, quantity, and quality of observational records (Knutson et al., 2020).

Although there has been a growing number of proxy records of paleo-

* Corresponding author. Department of Earth, Ocean, and Atmospheric Science, Florida State University, Tallahassee, FL, 32306-4520, USA.
E-mail address: ywang@magnet.fsu.edu (Y. Wang).

https://doi.org/10.1016/j.quascirev.2024.108710
Received 29 January 2024; Received in revised form 30 April 2024; Accepted 1 May 2024

hurricane activities from the western Atlantic region, relationships between the temporal and/or spatial variabilities in hurricane frequency and potential drivers remain ambiguous (e.g., Brandon et al., 2013; Bregy et al., 2018; Denommee et al., 2014; Donnelly et al., 2015; Donnelly and Woodruff, 2007; Ercolani et al., 2015; Lane et al., 2011; McCloskey and Liu, 2012; McCloskey and Liu, 2013; Muller et al., 2017; Muller et al., 2022; Rodysill et al., 2020; Schmitt et al., 2020; Sullivan et al., 2022; Wallace et al., 2021b). Furthermore, almost all existing paleo-hurricane records are based on documenting and dating sand overwash event beds (i.e., coarse-grained deposits) in sediment cores from coastal environments. Although the storm strength required for overwash and deposition varies among sites, studies of modern events and hydrodynamic modeling show that intense hurricanes (Category 2 or higher) passing nearby (within <100 km) are more likely to leave overwash event beds among deposits of fine mud and/or peat (Lin et al., 2014; Wallace et al., 2021b). Thus, these grain-size-based records, although valuable, greatly underestimate paleo-hurricane frequency (Das et al., 2013; Jahan et al., 2021; Lambert et al., 2008). This makes it difficult to detect significant changes in TC frequency affecting a site because lower magnitude hurricanes are not counted. Moreover, a recent study suggests that variation patterns of paleo-hurricane activity in single sediment records from a specific locality may reflect randomness (i.e., weather variability) rather than climate change (Wallace et al., 2021a). This highlights the importance of developing high-resolution records with good chronological control from more localities across a region. In addition, development of proxies that can capture lower magnitude hurricanes impacting a site will help to understand the possible links between the long-term spatiotemporal variability of TC activity and climatic forcing as well as improving climate model projections of TC activity for the future.

Here, we present a 5500-year-long, high resolution, multi-proxy TC record with robust chronology for the northeastern Gulf of Mexico (GOM) region. Our reconstruction is based on identifying and counting TC-induced flooding events using multiple organic geochemical proxies (OGPs) preserved in sediment cores from two coastal lakes ~170 km apart, Mullet Pond and Eastern Lake, in north and northwest Florida. Using two lakes should eliminate, or at least reduce, the potential sampling bias of individual sediment records (Wallace et al., 2021a). We then compare the TC record with published paleoclimate records, long-term solar variability, and other relatively high-resolution paleo--hurricane reconstructions from the western North Atlantic region. This allows us to examine the temporal and spatial patterns of hurricane activity and to test hypotheses regarding various potential drivers of North Atlantic TC variability.

2. Study area

Two coastal lakes Mullet Pond and Eastern Lake in the northeastern

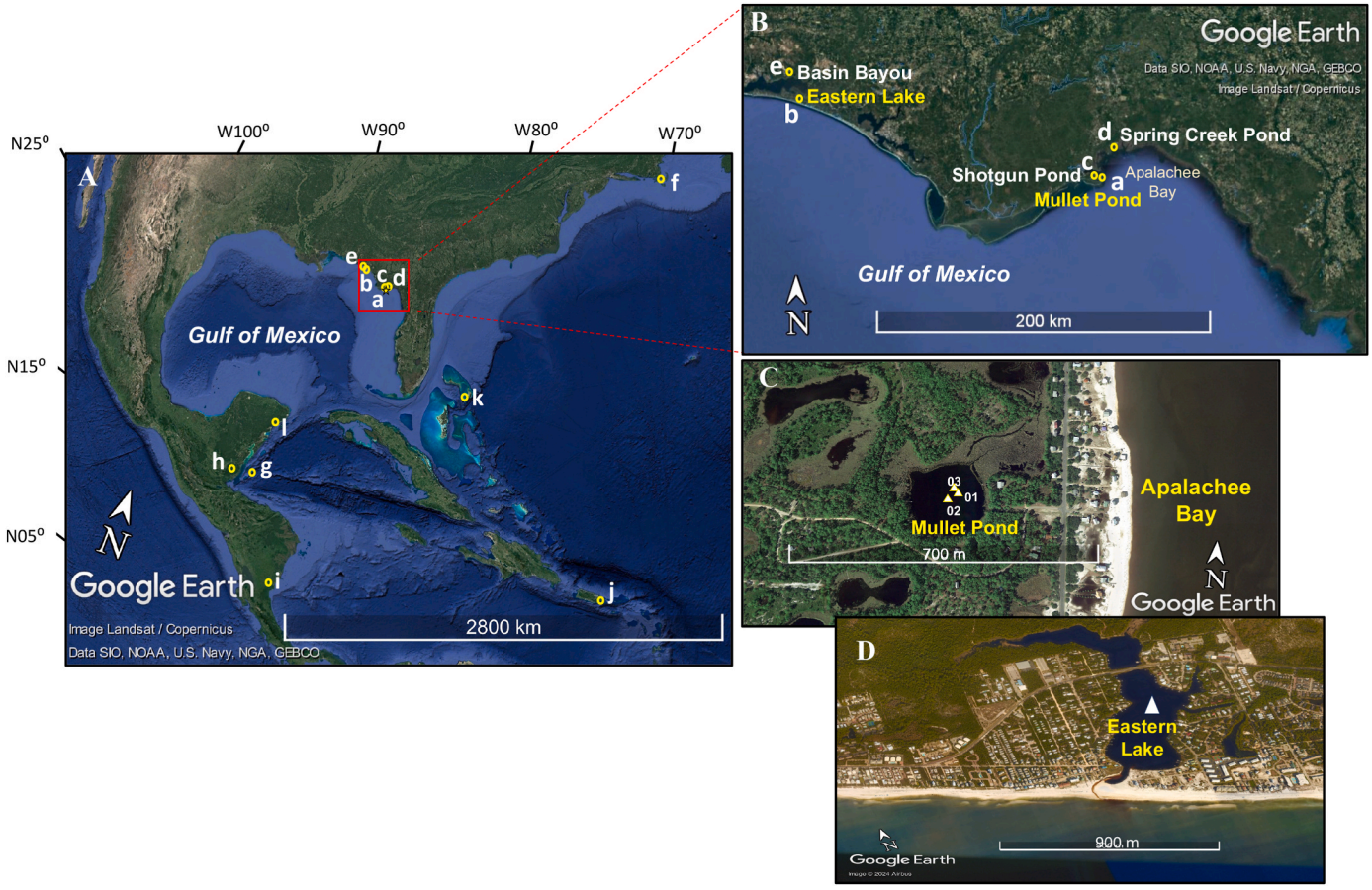

Fig. 1. Location Maps. Panels A and B show the locations of the two study sites and previously published paleo-hurricane records in the western Atlantic region discussed in the text: (a) Mullet Pond, FL (Lane et al., 2011) (this study); (b) Eastern Lake, FL (Das et al., 2013) (this study); (c) Shotgun Pond, FL (Rodysill et al., 2020); (d) Spring Creek pond, FL (Brandon et al., 2013); (e) Basin Bayou, FL (Rodysill et al., 2020); (f) Salt Pond, MA (Donnelly et al., 2015); (g) Lighthouse Reef, Belize (Schmitt et al., 2020); (h) Hopkins Swamp and Commerce Bight Lagoon, Belize (McCloskey and Liu, 2013); (i) Falso Bluff Marsh, Nicaragua (McCloskey and Liu, 2012); (j) Laguna Playa Grande, Vieques, Puerto Rico (Donnelly and Woodruff, 2007); (k) Blue Holes, The Bahamas (Wallace et al., 2021b), and (l) Cenote Muyil, northeast Yucatan (Sullivan et al., 2022). Panel (C) shows an aerial view of Mullet Pond with core locations (02 = MP052416-02B, 01 = MP120916-01B, 03 = MP120916-03A). Panel (D) shows an aerial view of Eastern Lake with core location. Base images were from Google Earth (Google Earth Pro 7.June 3, 9345, https://earth.google.com).

Gulf of Mexico region (GOM) were selected for this study (Fig. 1). Both lakes have been used in previous paleo-storm studies (Das et al., 2013; Jahan et al., 2021; Lane et al., 2011).

Mullet Pond (29°55.520′N, 84°20.275′W) is located in the Bald Point State Park along north Florida's Gulf Coast (Fig. 1). The area is underlain by hundreds of meters of limestone that is overlain by a layer of sand and clays (Puri and Vernon, 1964; Sinclair and Stewart, 1985). Dissolution of the underlying limestone by slightly acidic rainwater has produced many sinkholes and other karst features in the area (Sinclair and Stewart, 1985). Mullet Pond is a sinkhole lake formed when an underground cavity in limestone collapsed ~7000–8000 years ago (Lane et al., 2011). The lake is ~350 m west of the Apalachee Bay and separated from the ocean by a 3–4 m high beach dune ridge located approximately 200 m east of the lake (Fig. 1B and C). The land west of the dune ridge is relatively flat, with an elevation of 2–3 m relative to the North American Vertical Datum of 1988 (NAVD88). A tidal creek runs through a small salt marsh to the north of the lake and intermittently connects the lake to the open coast during high storm surges (Fig. 1C). The lake is about 2–3 m deep and is nearly circular, with a diameter of ~200 m. The surface salinity measured over a 3-year period (from May 2016 to November 2019) varied from 0.3 to 16.9 psu, with an average value of 9 ± 4 psu (Jahan et al., 2021).

Eastern Lake (30°18′41.857″ N, 86°5′35.647″ W) is located in Walton County on the northwest Gulf Coast of Florida (Fig. 1B). The lake occupies 2.8 ha and has an average water depth of ~3 m (Lakewatch, 2008). The underlying geology in this area consists of up to 33 m of undifferentiated quartz sand and clayey sand overlying the Miocene-Pliocene Intracoastal Formation, which consists of phosphatic, quartz sand and sandy carbonate (Schmidt, 1984). The area has well-developed coastal sand dunes that rise as much as 9 m in height, separating the lake from the Gulf of Mexico (Das et al., 2013). The average surface salinity of the lake water was 10.6 psu and the average pH was 7.5 for the period of 2001–2008 (Lakewatch, 2008). The lake has an outlet slough that temporarily connects it to the Gulf of Mexico during high water events (Fig. 1D).

3. Methods

3.1. Collection and description of sediment cores

We collected five sediment cores in 2016 near the center of Mullet Pond (Fig. 1C). These cores were collected using a hand-held piston corer in clear polycarbonate barrels (with an inside diameter of 68 mm), except for core MP120916-03A which is a 228 cm long vibracore and was collected in 3-inch diameter aluminum tubing. Coring tubes were held vertical to maintain sediment integrity while coring the sample from the lake bottom and afterward were sealed at both ends of the tubes to preserve core top structure. The clear core tubes of the short cores allow verification of core top integrity. The cores were transported to the Florida Geological Survey, where each core was split lengthwise into two halves. One half of each core was archived for future research and the other core halves were subjected to initial core analysis, including high-resolution imaging and lithologic descriptions. Based on these initial analyses, we selected three cores including MP052416-02B (100.5 cm long), MP120916-01B (64.25 cm long), and MP120916-03A (228 cm long) for detailed sampling for geochemical work.

The short cores are comprised of dark, organic-rich fine-grained sediment with no visible overwash sand layers (Suppl. Fig. 1). The upper 70 cm of the long core (MP120916-03A) contains similar dark, fine-grained sediment; the depth interval from ~70 cm to ~120 cm consists of dark, fine-grained material interbedded with sand lamina that varied in thickness. From ~120 cm to ~130 cm depth, the sediments are composed of dark, fine-grained material mixed with sand; and below ~130 cm, the core consists of light brown, organic-poor, medium to coarse grained quartz sand (Suppl. Fig. 1). The thick sand deposit below ~130 cm at the bottom of the long core is too thick (>1 m) to be an overwash deposit. The lithologic change from quartz sand to organic-rich sediment in the lower part of the long core most likely reflects a change in the local environment resulting from a collapse of an underground cavity and sandy overburden to form a lake.

3.2. Sampling and analyses of sediments

To optimize the ability to identify paleostorm horizons, each of the selected core halves was sliced into subsamples at closely spaced sampling intervals of ~0.25 cm. For the vibracore (MP120916-03A), only the lower (>38 cm), undisturbed section of the core was subsampled. A total of 402, 257, and 326 sediment samples were obtained from cores MP052416-02B, MP120916-01B, and MP120916-03A, respectively. These sediment samples were freeze-dried and then carefully inspected to pick out plant fragments for radiocarbon (^{14}C) dating before being ground and homogenized into a fine powder. Sediment samples from the upper 30 cm of core MP120916-01B were processed for ^{210}Pb dating to refine the ages of the most recent storm layers at this site. The ^{210}Pb methods, modeling and results are described in detail elsewhere (Burnett et al., 2023; Jahan et al., 2021).

Because the sediment samples did not contain any detectable amount of carbonate, they were directly weighed (~5 mg) and wrapped into tin cups for stable isotope analysis using a Carlo Erba Elemental Analyzer (EA) connected to a Finnigan MAT Delta Plus XP stable isotope ratio mass spectrometer at Florida State University. The isotope results are reported using standard delta (δ) notation in per mil as δ^{13}C values with reference to the international VPDB standard and δ^{15}N values with reference to AIR. The analytical precisions based on repeated analyses of laboratory standards (YWOMST-1, YWOMST-2, YWOMST-3, YWOMST-4, YWOMST-5 and Urea-2) were ±0.1‰ (1σ) for δ^{13}C and δ^{15}N, and ±0.2 (1σ) for C/N atomic ratios, respectively. Replicated analyses of our sediment samples, which have much lower N contents than the standards, suggest a lower precision of 0.4 (1σ) for C/N.

We also re-examined an archived half core EL052209-03 (Suppl. Fig. 1) previously analyzed for OGPs from Eastern Lake and reported in Das et al. (2013) to pick out plant fragments for ^{14}C dating and sampled the upper 20 cm for ^{210}Pb dating to improve the chronology of the OGP record.

Plant fragments (all terrestrial except one sample that may be aquatic) from sediment cores from both lakes were sent to the Keck Carbon Cycle AMS Facility at the University of California in Irvine for ^{14}C dating. Most of the ^{14}C data have been reported elsewhere (Jahan et al., 2021; Wang et al., 2019) but were re-calibrated using InterCal20 (Reimer et al., 2020) in this study (Suppl Table 1).

The Eastern Lake core (EL 052209-03) previously analyzed for OGPs (Das et al., 2013) was sub-sampled for this study at 1 cm intervals for ^{210}Pb dating. The moisture content of the sediment was determined previously by weighing, drying and a second weighing of the dry sediment. Bulk densities for each interval were calculated from the measured moisture content and an assumed average grain density of 2.5 g/cm^3. The activities of ^{210}Pb and ^{226}Ra were measured by direct gamma counting (46.5 keV for ^{210}Pb and 295 keV for ^{226}Ra) on 20 samples from the upper 20 cm of the core (Suppl Table 2). The "excess" ^{210}Pb activity is the activity above that supported by the long-lived parent ^{226}Ra present in the sediment. All excess ^{210}Pb activities were decay corrected back to the date of sediment collection after subtracting the estimated supported ^{210}Pb level. The supported level was estimated by averaging the measured activities of ^{226}Ra in the core. The Constant Rate of Supply (CRS) model (Appleby and Oldfield, 1978, 1992; Burnett et al., 2023) was used to calculate the ages of the sediment layers. We also used the Constant Flux, Constant Sedimentation (CF:CS) model (Appleby and Oldfield, 1978, 1992; Burnett et al., 2023) to estimate the average sediment accumulation rate (SAR), assuming a constant ^{210}Pb flux and a constant sedimentation rate.

3.3. Establishing core chronologies

Twenty-three ^{14}C dates were obtained from the three cores from Mullet Pond and ten additional dates from the Eastern Lake core (Suppl. Table 1). The ^{14}C ages of plant fragments generally increase with depth in each of the cores, with a few age reversals occurring near the top and at ~21 cm in core MP120916-01B, ~104 cm in MP120916-03A, and ~82 cm in EL052209-03 (Suppl. Table 1). Because radiocarbon age reversals in coastal lake sediment cores are most likely caused by deposition of pre-aged organic material eroded from land by large storm events (Wang et al., 2019), these few reversed ages were not used as control points in the age-depth models for the cores.

The ^{14}C dates on plant fragments from various depths in the cores were used as control points to develop age-depth models with 95%

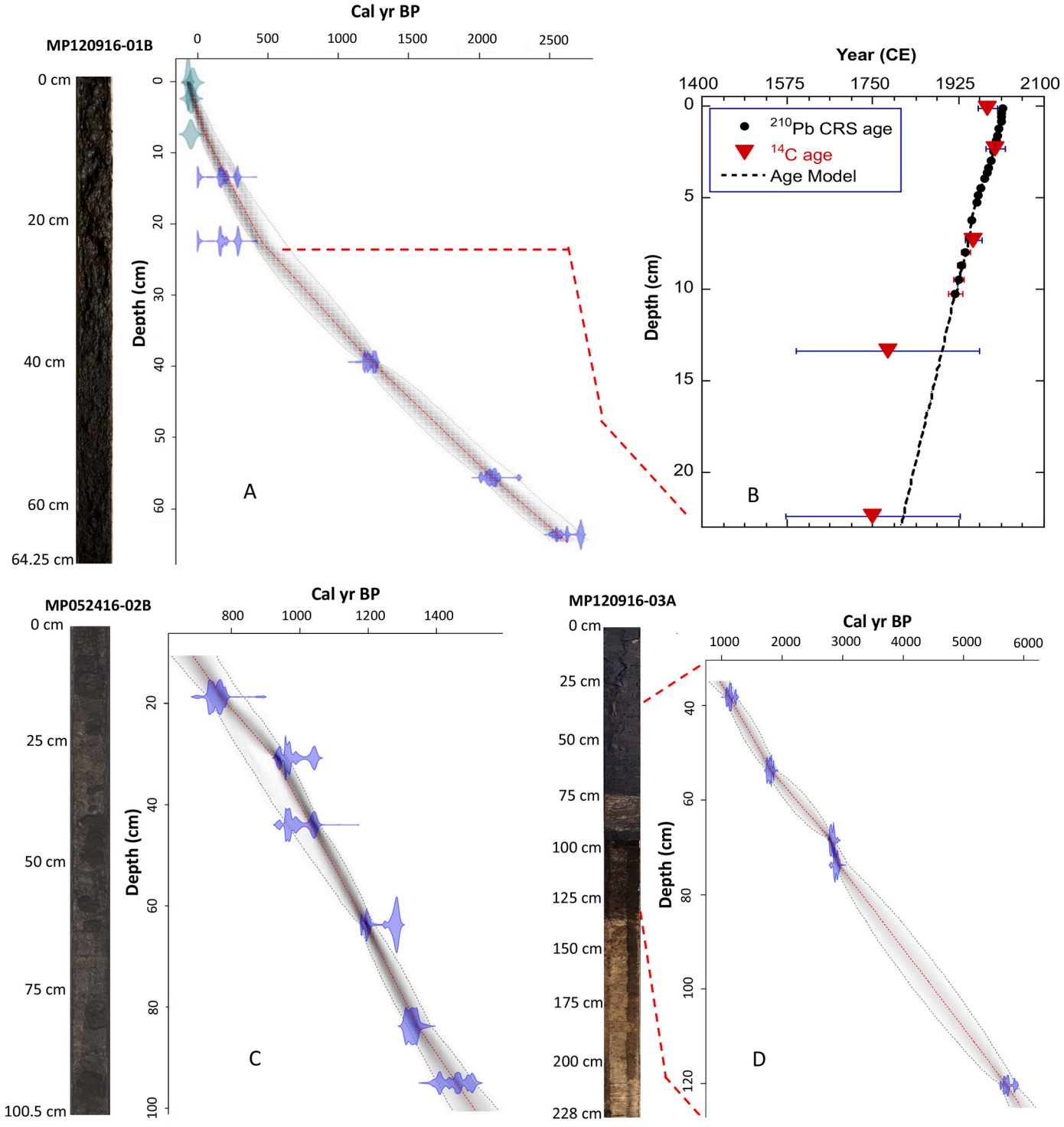

Fig. 2. Age model outputs from the Bacon model (Blaauw and Christen, 2011) for Mullet Pond sediment cores. Age models are constrained by ^{14}C ages of plant fragments found at various depths in the cores (A, C, D) and ^{210}Pb CRS ages from Jahan et al. (2021) (B) that provide a refined chronology for recent sediments. The weighted mean age-depth profile is indicated by a solid red line, calibrated ^{14}C age probabilities are shown in blue, and the black dotted lines bracketing the age-depth shaded curves indicate the 95% confidence interval. Error bars in (B) represent 2 standard deviations (2σ) from the mean.

confidence intervals for the cores using Bayesian statistical approaches in the R package Bacon v3.2.0 model (Blaauw and Christen, 2011). The Bacon model outputs with uncertainty envelope are shown in Figs. 2 and 3. A thick (~3 cm) sand layer in EL052209-03 was assumed to have been deposited instantaneously in the downcore age-model (Fig. 3). The age-depth models for the cores were refined with ^{210}Pb dating for the shallower depths (Figs. 2 and 3).

The three cores from Mullet Pond span different lengths of time and display similar geochemical patterns during time intervals when they overlap (Fig. 4). They were combined to develop a composite, long-term record, with the overlapping time intervals represented by core samples having the highest possible time-resolution (Suppl. Tables 3 and 4). The composite record covers the last 5700 years, with a mean sedimentation rate of 1.4 mm/yr (ranging from 0.1 to 9.5 mm/yr). The resulting resolution for the composite record ranges from 0.3 to 17.4 years per sample, with a median of 3.3 years per sample (Suppl. Table 3). The Eastern Lake core spans the last 2700 years, with a mean sedimentation rate of 0.5 mm/year (ranging from 0.1 to 1.6 mm/yr). The time resolution for the Eastern Lake record varies from 1.9 to 44.6 years per sample, with a median of 6.1 years per sample (Suppl. Table 5).

3.4. Detecting TCs in sediment cores using multiple OGPs

Earlier studies have shown that OGPs (δ^{13}C, δ^{15}N and C/N) are a more sensitive indicator of past storm events than traditional proxies used in paleotempestology as using multiple OGPs can detect seawater flooding events that may or may not deposit overwash sand in the lake (Das et al., 2013; Lambert et al., 2008). This is because organic matter (OM) of marine origin generally has higher δ^{13}C and δ^{15}N values but lower C/N ratios than those derived from terrestrial C_3 plants (Meyers, 1997). Furthermore, the seawater in the GOM has much higher concentrations of inorganic nutrients than coastal lake waters (Das et al., 2013; Lambert et al., 2008). An influx of marine nutrients due to seawater inundation can lead to a rapid eutrophication spike in the coastal lake after a storm. As a result, OM formed and deposited on the lake bottom under seawater "flooded" state would be more enriched in ^{13}C and ^{15}N than OM formed under the normal lake conditions (Lambert et al., 2008). A landfalling TC may cause seawater inundation of coastal lakes in the affected area if storm surges are high enough to breach or overtop the barrier dunes; it may also cause freshwater flooding due to associated heavy rainfall. In a recent study (Jahan et al., 2021), we further tested the validity of the multi-OGPs method for detecting TCs with modern time series data from two coastal lakes (including Mullet Pond) in north and northwest Florida as well as recent sediment core data from Mullet Pond. Our 3-year geochemical time series data show that the geochemical properties of these lakes varied seasonally, reflecting variations in lake biological and environmental conditions, but produced unique variation patterns in response to flooding events caused by large storms. This underscores the importance of using multiple geochemical proxies because the interpretation of any single geochemical proxy alone can be ambiguous. During the period when we collected modern data (2016–2019 CE), several major storms passed within 150 km of one or both lakes and caused influxes of either seawater and/or freshwater into the lakes, resulting in measurable changes in the δ^{13}C, δ^{15}N and C/N values of particulate organic matter (POM), along with changes in the salinity, δ^{18}O and δD of the lake water. Large storm events that cause seawater flooding (SW) tend to increase both the δ^{13}C and δ^{15}N values, with either a decrease or no change in the C/N ratios of the POM (Fig. 5). These observations support the previously proposed conceptual model for using multiple OGPs to identify SW events (Lambert et al., 2008). Our modern data also show that freshwater flooding (FW) decreases the δ^{15}N and increases the C/N values of POM but could also result in decreases in both δ^{15}N and δ^{13}C values, with little or no change in the C/N ratio (Fig. 5). Large storms that passed >150 km away from the study lakes had little or no effect on the physical and geochemical properties of these lakes. Our modern time

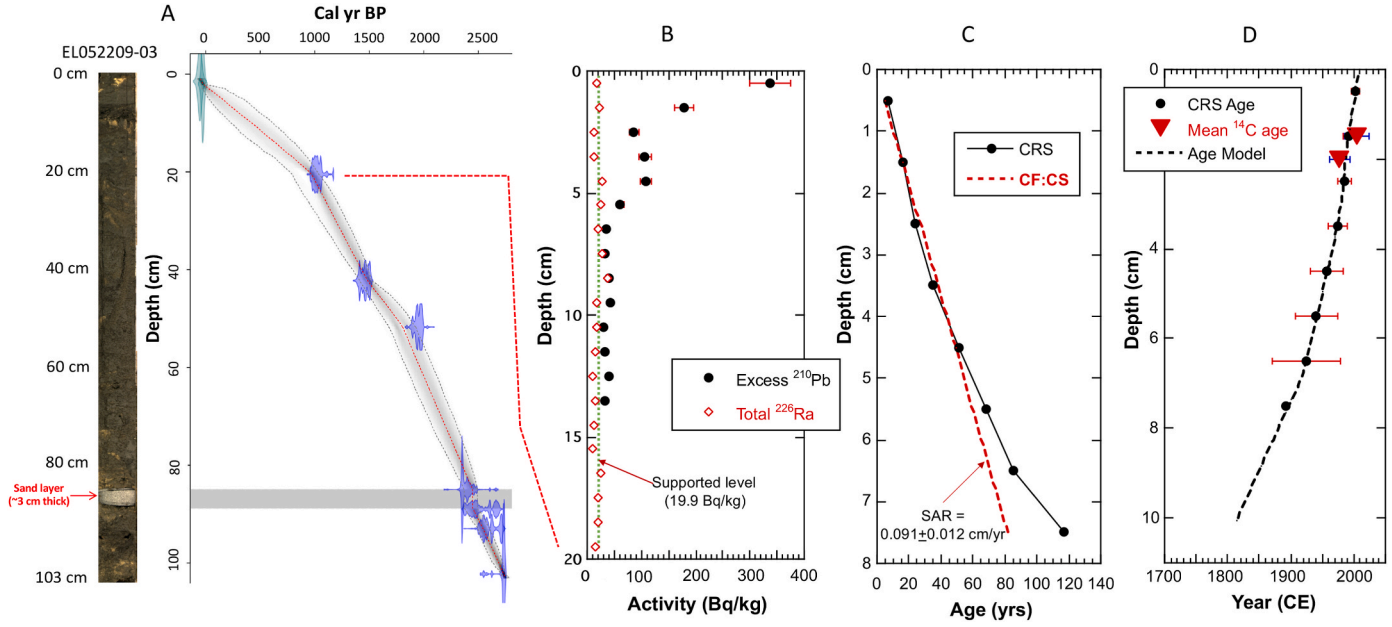

Fig. 3. Revised age model for core EL052209-03 from Eastern Lake in northwest Florida based on additional ^{14}C and new ^{210}Pb dating: (A) Age model outputs from the Bacon model (Blaauw and Christen, 2011), with the solid red line indicating the weighted mean age-depth relationships. The calibrated ^{14}C age probabilities are shown in blue, and the black dotted lines bracketing the age-depth shaded curves indicate the 95% confidence interval. (B) Activities of ^{226}Ra and excess ^{210}Pb in the upper 20 cm of the core (there is no excess ^{210}Pb below the 13 cm interval). (C) Ages (in years before sampling date) calculated from excess ^{210}Pb using the Constant Rate of Supply (CRS) model, along with the average sediment accumulation rate (SAR) calculated using the Constant Flux and Constant Sedimentation (CF:CS) model. (D) Age model based on ^{210}Pb CRS ages of sediment layers extrapolated to 10 cm depth in the core using the sedimentation rate determined from CRS ages. The previous age model was based on very limited ^{14}C dates from the 85–94 cm depth interval in the core, assuming a constant sedimentation rate throughout the entire core (Das et al., 2013). The new age model is constrained by 9 ^{14}C ages of plant fragments found at various depths in the core (A) and the ^{210}Pb CRS ages that provide a refined chronology for recent sediments (D). Error bars represent 2 standard deviations (2σ) from the mean.

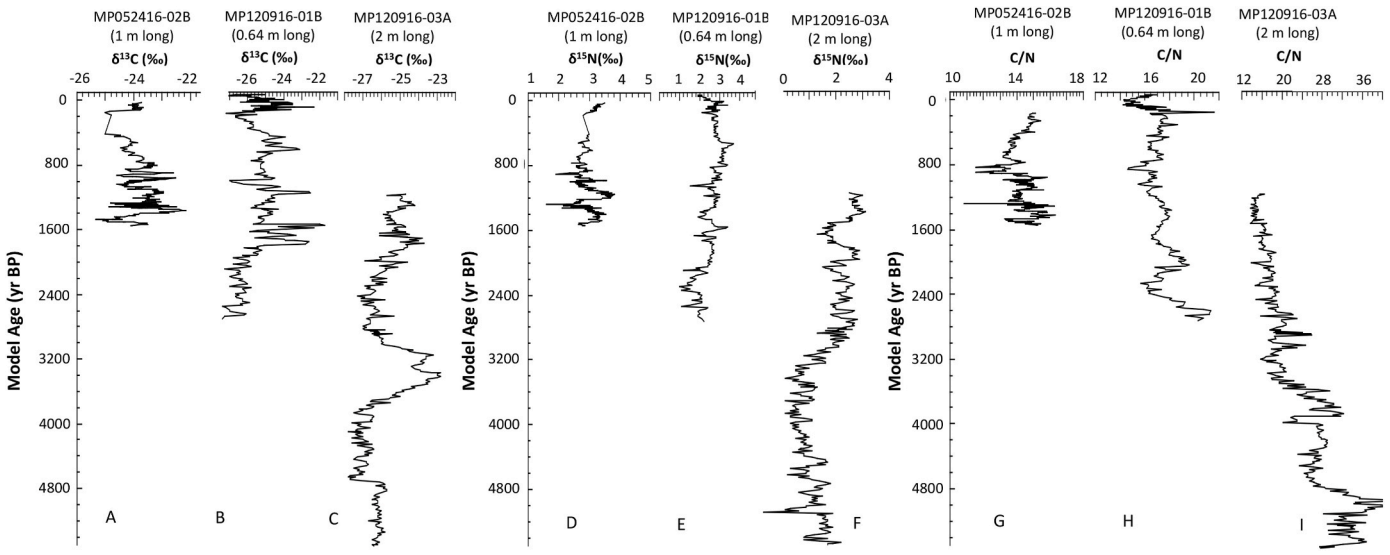

Fig. 4. Comparison of $\delta^{13}C$ (A–C), $\delta^{15}N$ (D–F), and C/N (G–I) profiles of three cores (MP052416-02B, MP120916-01B, and MP120916-03A) from Mullet Pond plotted against model ages. The three cores overlap in time and their geochemical proxies display similar patterns during intervals when they overlap.

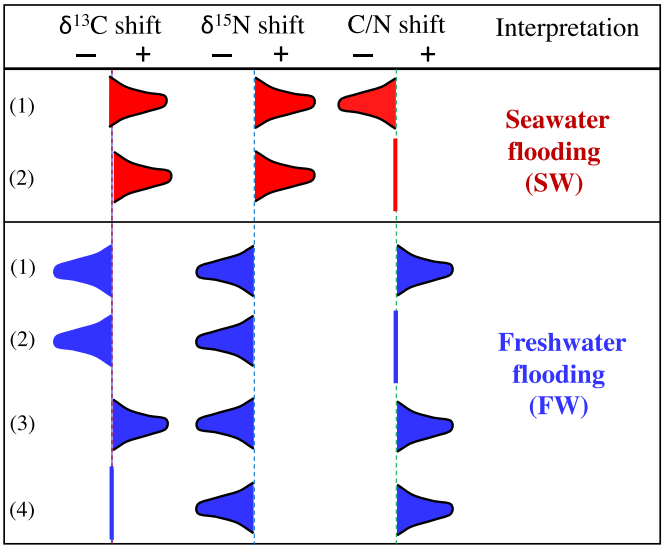

Fig. 5. Conceptual diagram of OGP interpretations (adapted from Fig. 7 in Jahan et al., 2021). The model shows that seawater flooding can result in two possible variation patterns of OGPs while freshwater flooding may lead to four possible OGP variation patterns as indicated by the numbers (1–2; 1–4). These multi-OGP variation patterns are used here as fingerprints to identify TC-induced SW and FW events in the sediment record.

series data demonstrate that it is feasible to detect both SW and FW events caused by large storms by examining variation patterns of multiple OGPs (Fig. 5). To further test the OGP method, we reconstructed a 165-year-long storm record based on variation patterns of $\delta^{15}N$, C/N and $\delta^{13}C$ preserved in the upper part of a sediment core (MP120916-01B) from Mullet Pond and compared the reconstruction with the documented storms that passed through the study lake area. The reconstruction reveals 30 flooding events, including 15 SW and 15 FW incidents, over the last 165 years (1850–2016 CE). Among these 30 flooding events, 28 were matched within dating uncertainties to historic hurricanes that are known to have passed within 150 km of the study site and the remaining 2 FW events detected in the OGP record correspond to tropical storms passing within 25 km of the lake (see details in Jahan et al., 2021). This provides confidence that these conceptual and observed variation patterns of multiple OGPs shown in Fig. 5 can serve as reliable fingerprints to identify TCs in sediment cores from Mullet Pond and other coastal lakes of similar environments (i.e., vegetated watersheds dominated by C3 plants).

Here we use this multi-OGPs approach (Fig. 5) to identify SW and FW events over a much longer sediment record from Mullet Pond to extend the TC record farther back in time. The geochemical data including $\delta^{13}C$ and $\delta^{15}N$ and C/N for the lake sediment were de-trended to remove any long-term trend using a first-order difference method by subtracting the next value from the current value to facilitate the identification of storm signals (Suppl Table 4). To facilitate comparisons between storm frequency during the instrumental record (1850–2016 CE) and event frequency in the paleorecords, we used a sliding window of 164 ± 4 years to calculate moving averages of TC frequency (events/century) by dividing the number of flooding events within the window by the width of the window and then multiplying by 100 (Suppl Table 4). We calculated average storm frequencies using both SW event counts and total (SW and FW) event counts. The resulting reconstruction of TC frequency extends back to ~5500 cal yr BP (Fig. 6A). Using the same approach and the new chronology (Fig. 3), we re-analyzed the OGP record previously published for Eastern Lake in northwest Florida (Das et al., 2013), ~170 km west of Mullet Pond, and calculated the SW and FW event frequencies (Fig. 6B; Suppl Table 5).

3.5. Statistical correlation analysis

To quantify the relationship between the TC frequency record from Mullet Pond and the total solar irradiance (TSI) record, we first converted the temporally non-uniform TC record to even intervals of 5 years (to be consistent with the sampling resolution of the TSI) using cubic spline interpolation (Fig. 7A). The resulting evenly distributed time series is less biased when analyzing statistical relationships. The interpolated data in this case show little or no difference from the original data.

Statistical parameters are typically calculated using non-decomposed data (e.g., the gray curves in the top panels of Fig. 7). However, this traditional approach often fails to reveal statistical relationships in cases when robust relationships only exist on certain timescales. Thus, we decomposed the interpolated TC data and TSI data into oscillatory components of varying amplitude and frequency (Fig. 7) using what is known as the "ensemble empirical mode decomposition" (EEMD) method (Wu and Huang, 2009). This allows us to analyze possible relationships that may exist between statistically dominant

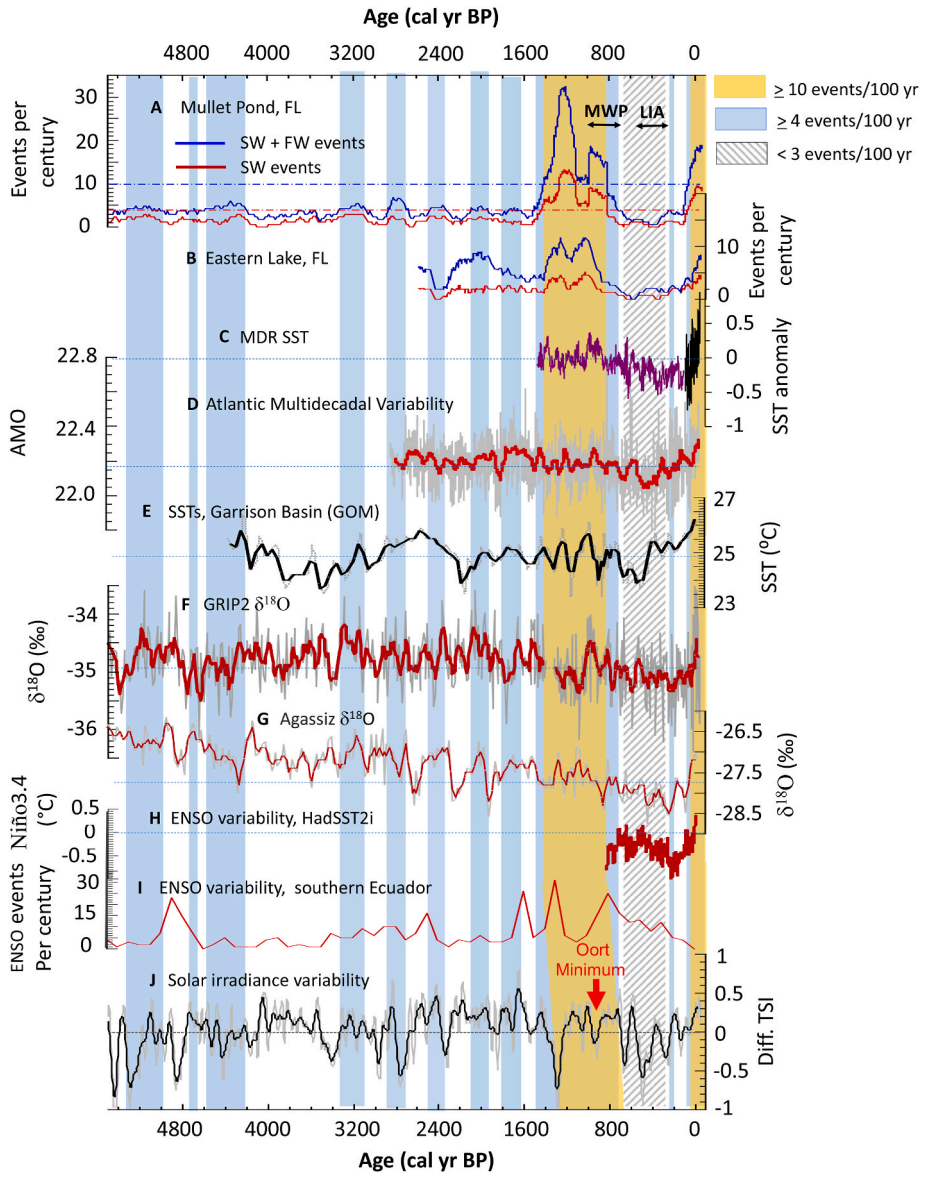

Fig. 6. Reconstructed TC frequencies in the northeastern GOM region and comparison to dominant indices of climate variability and solar output. (A) Reconstructed TC frequencies based on SW events (red) and combined SW and FW events (blue) detected in the sediment OGP record from Mullet Pond (FL) (this study). Horizontal red and blue dashed lines indicate the long-term average TC frequencies based on SW events (4 storms/century) and combined SW and FW events (10 storms/century), respectively. (B) Reconstructed TC frequencies based on SW events (red) and combined SW and FW events (blue) detected in the sediment OGP record from Eastern Lake (FL) (this study). Fewer storms were resolved from Eastern Lake, compared to Mullet Pond, due to the lower age resolution because of the combination of its slower sedimentation rate and sampling precision. (C) SST anomaly reconstruction (purple) and instrumental record (black) for the MDR for Atlantic TC (Mann et al., 2009a). (D) Proxy reconstruction of AMO, based on an annually laminated sedimentary titanium record from South Sawtooth Lake, Canada (Lapointe et al., 2020), with the red curve representing a 50-year running average. (E) SST record from Garrison Basin, northern Gulf of Mexico, derived from paired Mg/Ca-$\delta^{18}O$ measurements of foraminifers from sediment cores (Thirumalai et al., 2018), with the black curve representing 50(±8)-year running averages. (F) The $\delta^{18}O$ record from the GRIP2 ice core, with the red curve representing a 50-year running average (Stuiver et al., 1995). (G) The $\delta^{18}O$ record from the Agassiz ice core, with the red curve representing 60-year running averages (Vinther et al., 2009). (H) SST anomalies in the Niño-3.4 region estimated from a network of proxies in locations sensitive to ENSO (Emile-Geay et al., 2013). (I) Reconstruction of ENSO variability based on light-colored, clastic laminae in a sediment core from Lake Laguna Pallcacocha, Ecuador (Moy et al., 2002). (J) Reconstruction of total solar irradiance (TSI) variability based on measurements of cosmogenic isotopes (^{10}Be in ice cores and ^{14}C in tree rings), with "diff. TSI" standing for the difference of TSI from the PMOD composite during the solar cycle minimum of the year 1986 CE, with the black curve representing a 50-year running average (Steinhilber et al., 2012).

components of the two datasets (Bretherton et al., 1999; Huang and Wu, 2008; Wu and Huang, 2004) (Fig. 8). If the original time series consists of white noise (i.e., representing a random process with no discernible pattern or predictable structure), the EEMD results will be made up of sequential components of about double the period but half the energy (Wu and Huang, 2004; Huang and Wu, 2008). We see in Fig. 7 that the energy of sequential components is not reducing, implying that later EEMD components contain non-random information. Also, it can be seen from Fig. 7A that the 6th component nicely explains the two peaks in the TC data between 1500 and 500 cal yr BP. Thus, we focus our analysis on the 6th component of both datasets (Fig. 8).

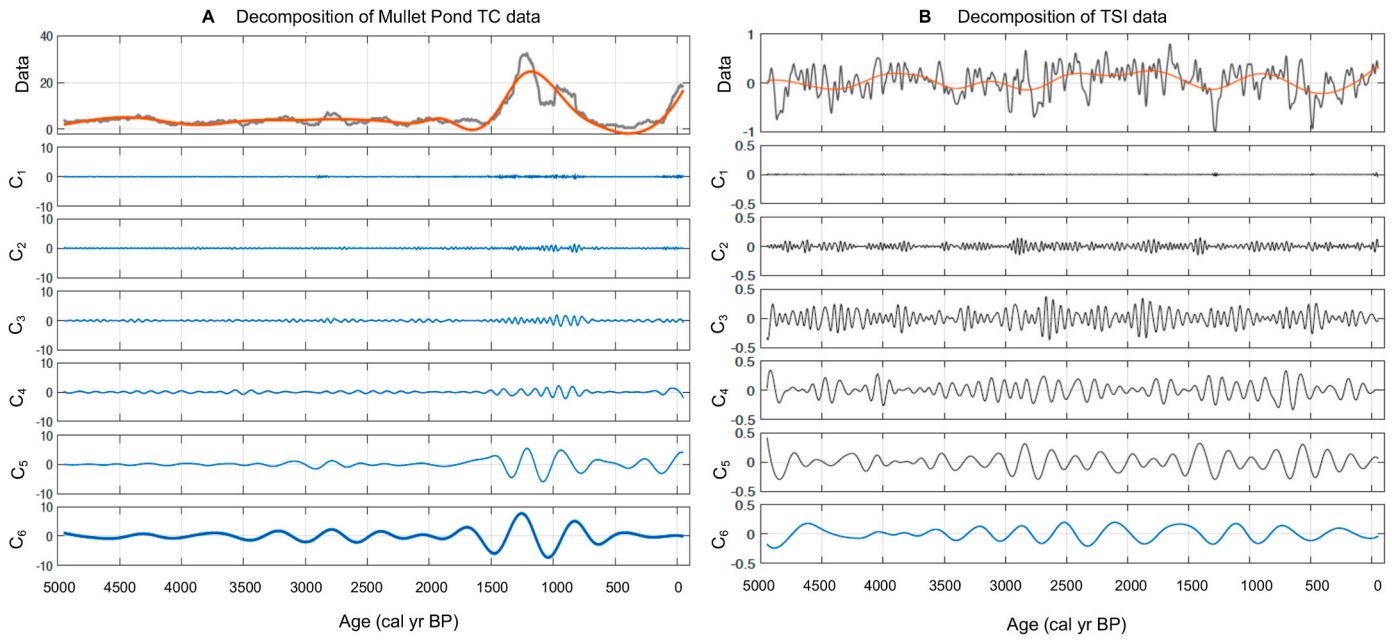

Fig. 7. EEMD analysis results showing the first 6 oscillatory components (C_1– C_6) of the Mullet Pond event frequency data (A) and TSI data (B). The top panel in (A) shows the interpolated version of the original event frequency data from Mullet Pond (gray) and the remainder of the data after removing the C_1– C_6 (red). The top panel in (B) shows the TSI data (gray) from Steinhilber et al. (2012) and the remainder of the data after removing the C_1– C_6 (red). The C_6 has a quasi-periodicity of ~400 years and is a statistically dominant component of both the TC frequency (based on Mullet Pond) and TSI records. The C_6 record also explains the two peaks of the TC record between 1500 and 500 cal yr BP.

4. Results and discussion

4.1. Temporal TC trends and relation to solar and climatic indices

Our new high-resolution, OGP-based paleo-storm record shows significant multi-decadal and centennial scale TC variability over the last 5½ millennia (Fig. 6A). It also reveals two active periods of TC strikes, from ~1410 to ~820 cal yr BP and from ~60 cal yr BP to the present, with both SW and FW event frequencies exceeding their long-term averages (shown as yellow bands in Fig. 6A). The pre-historic active period appears to correspond to a high solar-activity phase that is only briefly interrupted by the solar quiet phase during the Oort Minimum (Steinhilber et al., 2012) (Fig. 6A–J). This prolonged active period includes two hyperactive intervals (with TC frequency ≥40% above the long-term average) centered at ~1200 cal yr BP and ~900 cal yr BP, the younger phase falling within the Medieval Warm Period (MWP, 1000-700 cal yr BP) (Mann et al., 2009b). The storm activity of these hyperactive intervals either exceeded or was comparable to that seen today (Fig. 6A). A similar pattern is also observed in the OGP record from Eastern Lake (Fig. 6B). These two prehistoric hyperactive intervals roughly coincide with the two active ENSO intervals observed in a sedimentation-based proxy record from southern Ecuador (Moy et al., 2002) (Fig. 6 A-B, I). It is important to note that available ENSO reconstructions yield inconsistent results and most of them do not extend beyond the last millennium (Emile-Geay et al., 2013; Schneider et al., 2018). Of the few longer ENSO records, the reconstruction based on light-colored laminations in the sediments of Lake Pallcacocha in Ecuador (shown in Fig. 6I) is the most widely cited paleo-ENSO record although its reliability as a conclusive paleo-ENSO record has been questioned (Schneider et al., 2018).

These active periods can also be matched (within dating uncertainties) to intervals of elevated SSTs in the North Atlantic including the TC main development region (MDR) and in the GOM (Lapointe et al., 2020; Mann et al., 2009a; Thirumalai et al., 2018) as well as generally higher $\delta^{18}O$ values in the GRIP2 and Agassiz ice cores (Stuiver et al., 1995; Vinther et al., 2009) (Fig. 6A–G). Although it is not clear what role the AMO plays in modulating GOM TCs, the latter suggests a possible link to warm AMO phases as the ice core $\delta^{18}O$ record co-varies with the AMO index over the instrumental record, with increasing SST leading to higher $\delta^{18}O$ values, and thus may serve as a proxy for North Atlantic SST variability (Knudsen et al., 2010).

In addition to the active periods noted above, the OGP record reveals several other intervals of elevated storm activity alternating with relatively quiet periods (Fig. 6A). In total, 11 periods of relatively high TC frequency (≥4 events per century) are recognized in the OGP record (shown in blue bands in Fig. 6A), lasting from <80 years to >700 years. These intervals of increased storm activity can all be matched, within dating uncertainties (Fig. 2), to elevated SSTs, higher $\delta^{18}O$ values in the ice cores, increased ENSO activity and higher solar irradiance (Fig. 6). The OGP record also reveals an exceptionally quiescent period from ~650 to ~280 cal yr BP (with <3 events/100 years) that overlaps the Little Ice Age (LIA, 550-250 cal yr BP) (Mann et al., 2009b). This quiescent period detected in our OGP record corresponds to generally lower SSTs, fewer ENSO events, lower $\delta^{18}O$ values in the ice cores, and lower solar irradiance (Fig. 6).

Statistical correlation analyses show remarkable coherence between solar irradiance and our OGP record of TC activity (Figs. 7 and 8). Both TSI and OGP TC records have a statistically dominant EEMD component with a periodicity of ~400 years (i.e., the C_6 panel of Fig. 7). The same periodicity is also one of the prominent spectral peaks in the maximum entropy power spectrum of the tree-ring calibrated ^{14}C record - a proxy record for solar activity (USGS, 2000). The maximum correlation between the TSI and GOM TC records for the last 2000 years occurs at a lag time of about 135 years (Fig. 8), which is within the dating uncertainties of the Mullet Pond record (Fig. 2). This maximum correlation coefficient value is 0.76, indicating that the correlation between the two datasets is statistically robust at about the 98% confidence level.

4.2. Comparison with grain-size-based paleo-hurricane records

Our OGP-based TC reconstruction not only reveals more storms than grain-size-based reconstructions from the same lake and from other

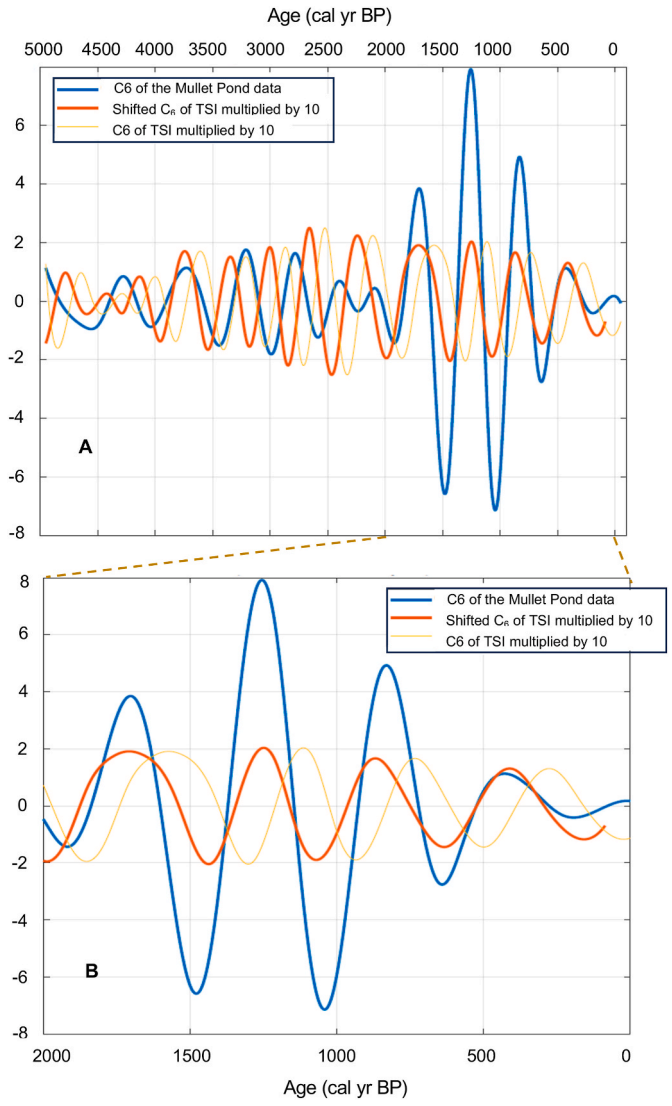

Fig. 8. Comparison of the 6th EEMD components (C_6) of the TC record from Mullet Pond (blue) and the TSI (orange) record. The red curve is the C_6 of the TSI record shifted in timing from the original C_6 curve (orange) by 135 years and aligns well with the C_6 of Mullet Pond data, especially for the most recent 2000 years. The maximum lag correlation between the two datasets for the last 2000 years occurs at a lag time of about 135 years which is within the dating uncertainties of the Mullet Pond record. The maximum correlation coefficient value at 0.76 indicates that the correlation between the two datasets is statistically robust at about 98% confidence level. Note that the amplitude of the C_6 of TSI is multiplied by 10 so that the two records have relatively close amplitudes.

lakes in the same region (Figs. 9 and 10) but also spans a much longer period, with finer time-resolution, than most paleo-hurricane proxy records (Fig. 10). Because ^{14}C dating of bulk sediment organic carbon generally yields unreliable ages (Wang et al., 2019), paleo-hurricane records with very low resolution or based on ^{14}C ages of bulk sediment organic carbon are not included for comparison, with the lone exception of the Lighthouse (Belize) paleo-record which has annual resolution and an age-depth model based on a combination of varve counting and ^{14}C dating of bulk sediment organic matter (Schmitt et al., 2020).

According to the NOAA best track data set (www.NOAA.gov), 35 hurricanes (including 23 Category 1, 8 Category 2, and 4 Category 3 storms) passed within 150 km of Mullet Pond from 1850 to 2016 CE. Among these 35 hurricanes, 19 can be matched with 15 SW events and the other 16 to 13 FW events identified in the OGP record (Fig. 9A). In comparison, the post-1850 CE grain-size anomaly record from the same lake detected only 7 overwash events that could be matched to 8 historic hurricanes (Fig. 9B and C) (Lane et al., 2011). Most of these events detected in the grain-size records matched SW events in the OGP record, except for the 2005 CE hurricane Dennis and 1985 CE hurricanes Elena/Kate that were matched within dating uncertainty to FW events identified in the OGP record (Fig. 9). This suggests that the influx of terrestrial OM into the lake, triggered by flooding in the lake's watershed from the very heavy rainfalls associated with hurricanes Dennis and Kate/Elena, may have overwhelmed the surge-driven marine OM input into the lake. The maximum surge heights of these storms estimated using the SLOSH (Sea, Lake and Overland Surges from Hurricanes) model were at least 1 m (above NAVD88) (Lane et al., 2011). Hydrodynamic modeling studies in the area show that 1.3–3 m storm surges could cause seawater inundation of Mullet Pond through a small tidal inlet ~0.5 km north of the lake but only storm surges exceeding 3 m, most likely driven by intense hurricanes (≥Cat. 2) passing nearby, have the potential to breach the dune barriers (~4 m above NAVD88) in front of Mullet Pond to cause overwash deposition in the lake (Lin et al., 2014). Based on hydrodynamic modeling results, Lin et al. (2014) noted that "*none of the historical surges dating back to the early nineteenth century likely exceeded the height of the modern barrier at Bald Point*" where Mullet Pond is located. This is consistent with the lack of visible sand layers in the younger portion of our sediment cores (Suppl. Fig. 1). Lin et al. (2014) interpreted the few event beds identified in the grain-size anomaly record from Mullet Pond during the recent historical interval (Fig. 9B and C) as the result of localized overwash and sediment transport *"likely facilitated by perpendicular cuts in the crest of the barrier for driveways of the homes located on the barrier"*. As shown in Fig. 9, both the OGPs and grain-size records from Mullet Pond are unable to resolve events that occurred closely in time. Although both types of proxies underestimate the number of TCs passing through the area, this shows that OGPs are a much more sensitive recorder of storm events than the grain-size proxy. OGPs detected ~83% of the documented hurricanes in the post-1850 CE era, while the grain-size record detected only ~20% of these documented storms (Fig. 9). Our OGP record from Mullet Pond suggests that the TC frequency during the post-1850 CE era is 6.3 events/century based on SW events and 13.8 events/century when both SW and FW events were considered, much higher than the estimates based on grain-size analysis of sediment cores from the same lake (Table 1). These numbers are also much higher than the estimates based on grain-size analyses from other lakes in the same region (Fig. 10C–F) but closer to those derived from the NOAA best track data (Table 1).

There are some similarities and differences in the long-term temporal TC pattern among the reconstructions (Fig. 10). The double-peaks seen by OGPs in both the Mullet Pond and Eastern Lake cores (Fig. 10A and B) also appear in the grain-size-based reconstruction from Mullet Pond (Fig. 10C), Shotgun Pond (Fig. 10D), Bahamas (Fig. 10G), and Salt Pond (Fig. 10H). While some time shifting is necessary for these peaks to be truly coincident, the similarity in the trends of these peaks from different areas is striking. Eastern Lake shows a higher frequency of TCs than Mullet Pond in the interval ~2200-1800 cal yr BP, perhaps because of its more exposed position along an open shoreline. The prolonged period ~1500-720 cal yr BP of increased TC activity identified in our OGP record roughly corresponds to a period of increased overwash events in the grain-size-based reconstructions from the same region (Fig. 10C–F) as well as other western Atlantic localities (Fig. 10G–J). The double peaks of this extended active period in our OGP records can be matched, within <250 years, to the twin peaks in the grain-size-based reconstructions of intense hurricane landfalls from the western Atlantic region (Fig. 10 A-D, G-H). The record from Shotgun Pond located ~2 km west of Mullet Pond matches particularly well (Fig. 10D). Some of the mentioned apparent differences may be due to regional effects. The higher TC frequency in the OGP record is likely due to the OGPs capturing lower intensity storms not detected by grain-size analysis. Our

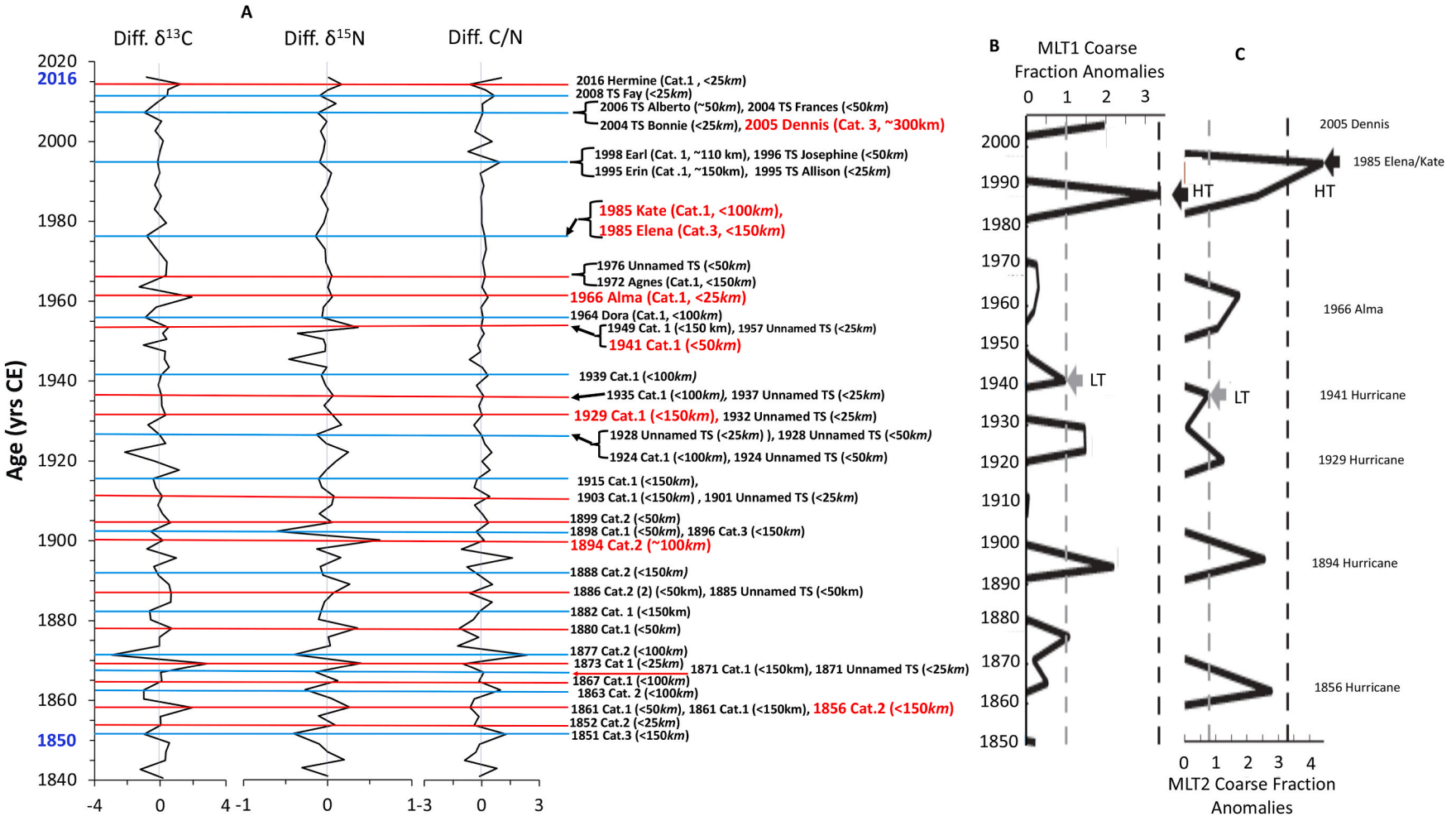

Fig. 9. Comparison of the OGP and grain-size based TC reconstructions from Mullet Pond for the post-1850 CE era. Panel A (adapted from Fig. 8 in Jahan et al., 2021) shows the de-trended OGP profiles, with red and blue lines marking SW and FW events, respectively, which were identified using multiple OGPs and the criteria shown in Fig. 5. Panels B and C (adapted from Fig. 5 in Lane et al., 2011) show the positive coarse grain fraction anomalies in cores MLT1 and MLT2, respectively, which were interpreted as overwash deposits resulting from storm surges caused by hurricanes listed on the right side of the figure. Gray and black dashed lines in B and C mark the low threshold (LT) and high threshold (HT) used by Lane et al. (2011) for storm detection. Also shown in (A) is the list of hurricanes (with their intensities and distances at closest approach to the study area) that passed <150 km from the lake as well as tropical storms (TS) that came ashore within 50 km of the lake (except for the 2005 CE Hurricane Dennis which passed ~300 km away from the lake), with the storms identified in the grain-size record highlighted in red.

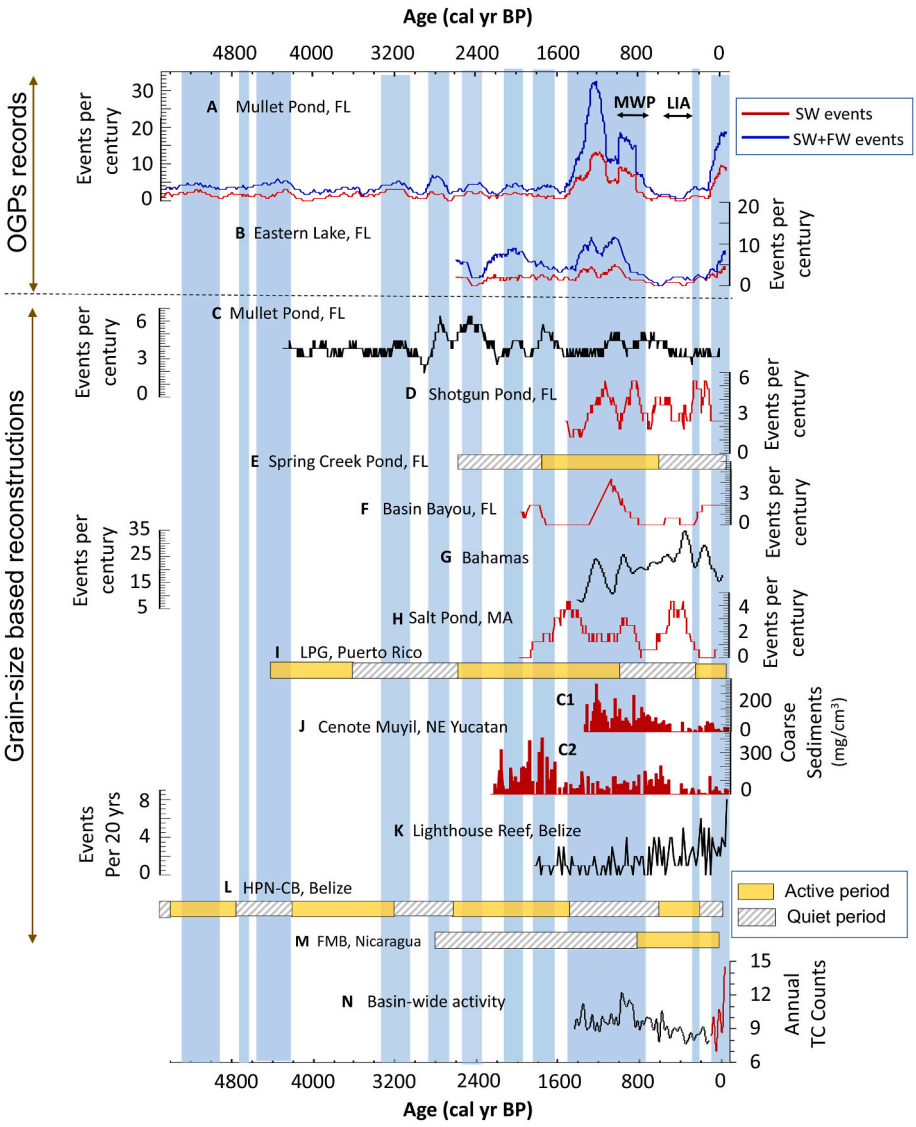

Fig. 10. Comparison of reconstructed TC frequencies based on multi-OGPs in sediment cores from Mullet Pond (A) (this study) and Eastern Lake (B) (this study) with grain-size-based reconstructions of intense-hurricane-induced overwash event frequencies from: (C) Mullet Pond (Lane et al., 2011), (D) Shotgun Pond (~2 km west of Mullet Pond) (Rodysill et al., 2020); (E) Spring Creek Pond (~20 km north of Mullet Pond) (Brandon et al., 2013); (F) Basin Bayou (~200 km west of Mullet Pond, ~23 km northwest of Eastern Lake) (Rodysill et al., 2020); (G) the Bahamas (Wallace et al., 2021b); (H) Salt Pond in Falmouth, MA (Donnelly et al., 2015); (I) Laguna Playa Grande (LPG), Vieques, Puerto Rico (Donnelly and Woodruff, 2007); (J) Coarse sediment (>63 mm) content, a proxy for TC event bed, for two cores C1 and C2 from Cenote Muyil in the northeast Yucatan (Sullivan et al., 2022). (K) Blue Hole on Lighthouse Reef, Belize (Schmitt et al., 2020); (L) the Hopkins Swamp and Commerce Bight Lagoon (HPN-CB), Belize (McCloskey and Liu, 2013); and (M) the Falso Bluff Marsh (FBM), Nicaragua (McCloskey and Liu, 2012). Also shown in (N) are smoothed modern annual Atlantic TC counts (red) and statistical model estimates of basin-wide TC counts from 1450 to 100 cal yr BP(black) (Mann et al., 2009a). Blue-shaded columns mark the intervals with increased storm activity identified in the OGP record from Mullet Pond.

Table 1
Comparison of average TC frequency derived from OGPs in sediment cores from Mullet Pond with those derived from grain-size analysis from the same lake (Lane et al., 2011) and the documented hurricanes from the NOAA database (https://coast.noaa.gov/hurricanes/).

Time period	OGP record		Grain-size record		NOAA best track record of TCs (≥Cat. 1)[c]	
	SW events per century[a]	(SW + FW) events per century[a]	HT events per century[b]	LT events per century[b]	TCs per century (100 km)	TCs per century (150 km)
Post-1850 CE	6.3	13.8	0.6	3.8	12.1	21.1
4500 Cal yr BP - present	4.6	10.7	2.4	3.9		
5500 Cal yr BP – present	4.4	10.1				

[a] SW and FW denote seawater and freshwater flooding events, respectively.
[b] HT and LT denote High-Threshold (≥Cat. 3) and Low-Threshold (≥Cat. 1) events, respectively, as defined in Lane et al. (2011).
[c] Documented storms passing within 100 km and 150 km of the study lake from 1850 to 2016CE.

reconstructions, however, differ substantially from the versions from Belize and Nicaragua in both the timing and lengths of the active and quiet periods (Fig. 10A–K-M). For the past 1600 years, the OGP records appear to show an opposite pattern to those observed in Belize and Nicaragua except for the modern era in which both the Lighthouse Reef record from Belize (Fig. 10K) and our OGP records see higher TC frequency. These differences are likely due to regional differences in TC activity but may also reflect chronological uncertainties of the individual paleo-records.

In the present-day climate, the Bermuda High (BH), the "south pole" of the NAO, exerts a steering control on TC tracks (Elsner et al., 2000; McCloskey et al., 2013). Given the steering effect of the BH, it has been hypothesized that the NAO is a major driver of TC activity over millennial timescales by affecting storm locations, such that a southward shift in the long-term position of the BH during cooler periods would drive storms southward, resulting in relatively more TC landfalls in the Caribbean region and relatively fewer landfalls at higher latitudes (Elsner et al., 2000; McCloskey et al., 2013). However, additional (non-paleo) studies (Kossin et al., 2010; Kozar et al., 2012) exploring the NAO and the BH have not found a consistent relationship between these features and the frequency of TCs impacting the western Caribbean/GOM, suggesting an interaction between the effects on hurricane steering and the effects on hurricane frequency. Furthermore, the increased hurricane landfalls during the LIA in the Bahamas and New England as suggested by grain-size records (Fig. 10G and H) and the inconsistent paleo-hurricane reconstructions from the Caribbean (Fig. 10I–M) underscore the complexity of unraveling the BH-NAO steering mechanism.

Our OGP-based storm record has a higher density of age control points than most earlier paleo-hurricane records. For example, the time interval from ~2000 cal yr BP to the present in our OGP record from Mullet Pond is constrained by 15 ^{14}C dates on plant fragments and refined with ^{210}Pb dating of sediments in the uppermost 30 cm of the core at 0.25 cm intervals (Fig. 2). In comparison, the same period in the grain-size paleo-hurricane record from the same lake (Lane et al., 2011) (Fig. 10C) was constrained by only 7 ^{14}C dates, along with fewer ^{210}Pb measurements for the upper 40 cm of their core at intervals ranging from 1 to 5 cm. The composite paleo-hurricane record from the HPN-CB site in Belize (Fig. 10L) had only 9 ^{14}C dates (for 8 sediment cores) over the last 5500 years (McCloskey and Liu, 2012) without any supporting ^{210}Pb dates. Besides the analytical errors associated with radiometric dates, inadequate age control points contribute additional uncertainties to age-depth models of sediment cores because sedimentation rates vary spatially and temporally even within the same lake (Wang et al., 2019). Fewer age control points would naturally result in larger errors in an age-depth model. It is thus important to keep in mind that uncertainties in the age models of individual paleo-records are larger than the uncertainties associated with individual ^{14}C ages that were used as controls in the age models of individual paleo-records (Fig. 10). Although regional differences in TC frequency pattern likely exist, the discrepancies among paleo-records (Fig. 10), at least in part, reflect the uncertainties in the age models used in the different studies as well as differences in the sampling resolution between different paleo-hurricane studies.

Our high-resolution OGP-based TC records from the northeastern GOM region display features similar to a 1500-year reconstruction of basin-wide Atlantic TC activity using a statistical model driven by proxy-based large-scale climate reconstructions (Mann et al., 2009a) (Fig. 10N). These records all show enhanced storm activities during the MWP and recent times as well as greatly reduced activities during the LIA (Fig. 10 A-B, N). The high TC activity during the MWP was thought to result from the reinforcing effects of La Niña-like climatic conditions and relative Atlantic warmth (Mann et al., 2009a). However, a paleo-temperature reconstruction from the eastern equatorial Pacific indicates that the MWP was a warm period in that region, contradicting the paradigm of a persistent La Niña state during the MWP (Rustic et al., 2015).

4.3. Potential drivers of long-term TC variability

Sea level in the northern Gulf of Mexico has been rising slowly over the last several millennia, resulting in a gradual landward migration of the shoreline (Milliken et al., 2008). This would increase the sensitivity of the study site to storm-surge-driven seawater inundation over time. However, it is difficult to assess the degree to which this change in site sensitivity to storm surge might have contributed to the increased SW event frequencies in recent times and during the prolonged prehistoric active period (~1500-720 cal yr BP) (Fig. 6A). The observed relationships between TC frequency and paleoclimate indicators and long-term solar variability (Figs. 6–8) underscore the importance of large-scale climatic and solar patterns in modulating TC strikes in the northeastern GOM region during the late Holocene.

Given the well-documented relationships between TCs and ENSO in the modern climate (Gray, 1984), it has been hypothesized that the frequency of intense hurricanes over the last millennia was modulated by atmospheric dynamics associated with variations in ENSO and the strength of the West African Monsoon (Donnelly and Woodruff, 2007). However, others argue there is no clear association between enhanced ENSO activity and TC activity that is consistent with modern relationships (Muller et al., 2017). Hurricanes impacting our study area over at least the last 150 years are mostly associated with strong ENSO (Suppl Fig. 2), suggesting that local storm activity is closely linked to variations in large-scale processes affecting the atmosphere-ocean system. In addition, SST variations in the tropical Atlantic related to the AMO are thought to drive TC activity, with more hurricanes forming during warm phases than cold phases of the AMO (Goldenberg et al., 2001). Comparison of our TC reconstruction with paleo-climate records confirms that warm SSTs in the tropical North Atlantic are a key ingredient for fueling TC activity in the Atlantic region (Fig. 6A–D, F-G). However, SSTs in the northern GOM, along with ENSO, appear to exert additional controls on storm activities in the northeastern GOM (Fig. 6A–E, H-I) since periods with SSTs as high as modern in the North Atlantic did not always support increased TC frequency in the GOM region (Fig. 6A–D, F-G). SST in the northern GOM is influenced by the Loop Current that brings warm waters from the Caribbean Sea into the GOM (Thirumalai et al., 2018). Loop Current transport is linked to seasonal migration of the Intertropical Convergence Zone (ITCZ) with the average position of the ITCZ varying in response to solar variability on centennial and millennial timescales (Nurnberg et al., 2008). Higher solar output would thus result in a more northerly position of the ITCZ, which would lead to a strengthened Loop Current and a warmer SST in the northern GOM (Thirumalai et al., 2018). Eleven periods of elevated TC activity over various time scales, with accompanying enhanced solar irradiance, are recognized in our OGP record (blue zones in Figs. 6 and 10). This statistically robust coherence of enhanced TC activity with higher solar irradiance (Figs. 7 and 8) supports the concept that solar activity may be an important driver of climate variability and TC activity through its influence on atmospheric circulation, ocean currents and SSTs (Ineson et al., 2011; Trouet et al., 2016; USGS, 2000).

Solar variability plays a complex role in modulating TC activity. Increased solar irradiance contributes to warming the oceans, resulting in larger areas with favorable SSTs for TC development. However, increased solar irradiance also warms the upper atmosphere, reducing the vertical temperature gradient in the troposphere. This not only weakens the vertical motion inside a developing TC (Hodges et al., 2014), but also causes shifts in atmospheric circulation (Haigh, 1996; Ineson et al., 2011). Although the responses of ENSO and other climate factors to solar forcing remain poorly understood, our findings suggest that a combination of high solar irradiance, enhanced ENSO activity, warm GOM SSTs, and positive AMO phases create favorable conditions for TC formation on multi-decadal and longer time scales in the northeastern GOM (Fig. 6).

5. Summary and conclusions

We summarize below our main conclusions together with the most relevant supporting information.

- Our multi-OGP-based high-resolution paleo-storm record indicates that the northeastern GOM region has experienced various TC activity regimes during the late Holocene. Over the last 5500 years, we recognize 11 relatively active periods (≥4 events/century), lasting from <80 years to >700 years. See data presented in Fig. 6A/B with highlighted intervals of relatively high TC frequency.
- A prolonged active period ~1500-720 cal yr BP comprises two hyperactive intervals centered at ~1200 cal yr BP and ~900 cal yr BP, with TC activity either exceeding or comparable to that seen today. One of these prehistoric hyperactive intervals coincides with the MWP. See data presented in Fig. 6A/B that clearly shows a prolonged active period that contains two hyperactive intervals, with the younger phase falling within the MWP.
- Our record also reveals a nearly 90% reduction in TC frequency relative to modern occurrences during a particularly quiet period from 650 to 280 cal yr BP that broadly corresponds to the LIA (see Fig. 6A/B and Suppl. Table 4).
- Our results suggest that warm SST in the tropical North Atlantic is a necessary but not sufficient condition for fueling TC activity in the northeastern GOM (see Fig. 6 that compares our TC reconstruction with published paleoclimate proxy records and long-term solar variability).
- High solar irradiance and warm GOM SSTs, coupled with increased ENSO activity and positive AMO, appear to create favorable conditions for enhanced TC activity on multi-decadal and centennial timescales in the northeastern GOM during the late Holocene. This is supported by the data (Fig. 6A–J) showing increased storm activity can all be matched, within dating uncertainties, to elevated SSTs (in both the North Atlantic and northern GOM), generally higher $\delta^{18}O$ values in ice cores (a proxy for AMO), increased ENSO activity, and higher solar irradiance. In addition, our EEMD and statistical correlation analysis (Figs. 7 and 8) show a very robust coherence between solar irradiance and our TC paleo-record.

Based on these findings, we suggest that improved future TC projections will depend upon a more advanced understanding of the complex responses of large-scale atmospheric/oceanic factors to radiative forcing. Our study also highlights the need to improve sampling, detection and dating resolution to elucidate the long-term spatiotemporal variation patterns of TC activity and their links to regional and global scale climate forcing.

CRediT authorship contribution statement

Yang Wang: Conceptualization, Methodology, Formal analysis, Writing, Funding acquisition. **Shakura Jahan:** Formal analysis, Formal analysis, Writing – review & editing. **William C. Burnett:** Conceptualization, Formal analysis, Writing. **Zhaohua Wu:** Formal analysis, Writing. **James B. Elsner:** Reviewing and Commenting. **Guy H. Means:** Assisting with sample collection, Reviewing and Editing. **Jin Liu:** Formal analysis, Reviewing and Commenting. **Shijun Jiang:** Sample analysis, Reviewing and Commenting.

Declaration of competing interest

The authors declare that they have no known competing financial interests or personal relationships that could have appeared to influence the work reported in this paper.

Data availability

All data produced in this study are reported in Supplementary Tables 1-5 as Appendix B. We also plan to submit our data to the NOAA Paleoclimatology online database after our paper is published.

Acknowledgments

This study was supported by a grant from the U.S. National Science Foundation grant EAR1566134 (YW). Sample preparation and stable isotope analyses were performed at the National High Magnetic Field Laboratory, which is supported by National Science Foundation Cooperative Agreement No. DMR-1644779 and the State of Florida. We are grateful to the anonymous reviewers for their constructive advice and comments.

Appendix C. Supplementary data

Supplementary data to this article can be found online at https://doi.org/10.1016/j.quascirev.2024.108710.

References

Appleby, P., Oldfield, F., 1978. The calculation of lead-210 dates assuming a constant rate of supply of unsupported 210Pb to the sediment. Catena 5, 1–8.
Appleby, P., Oldfield, F., 1992. Applications of lead-210 to sedimentation studies. In: Ivanovich, M., Harmon, R.S. (Eds.), Uranium-series Disequilibrium: Applications to Earth, Marine, and Environmental Sciences, second ed. Clarendon Press, Oxford (United Kingdom), pp. 731–783.
Blaauw, M., Christen, J.A., 2011. Flexible paleoclimate age-depth models using an autoregressive gamma process. Bayesian Analysis 6, 457–474.
Brandon, C.M., Woodruff, J.D., Lane, D.P., Donnelly, J.P., 2013. Tropical cyclone wind speed constraints from resultant storm surge deposition: a 2500 year reconstruction of hurricane activity from St. Marks, FL. Geochem. Geophy. Geosy. 14, 2993–3008.
Bregy, J., Wallace, D., Minzoni, R.T., Cruz, V., 2018. 2500-year paleotempestological record of intense storms for the northern Gulf of Mexico, United States. Mar. Geol. 396, 26–42.
Bretherton, C.S., Widmann, M., Dymnikov, V.P., Wallace, J.M., Bladé, I., 1999. The effective number of spatial degrees of freedom of a time-varying field. J. Clim. 12, 1990–2009.
Burnett, W., Bidorn, B., Wang, Y., 2023. Can 210Pb be used as a paleo-storm proxy? Quat. Sci. Rev. 315, 108242.
Das, O., Wang, Y., Donoghue, J., Xu, X.M., Coor, J., Elsner, J., Xu, Y.F., 2013. Reconstruction of paleostorms and paleoenvironment using geochemical proxies archived in the sediments of two coastal lakes in northwest Florida. Quat. Sci. Rev. 68, 142–153.
Delworth, T.L., Mann, M.E., 2000. Observed and simulated multidecadal variability in the Northern Hemisphere. Clim. Dynam. 16, 661–676.
Denommee, K.C., Bentley, S.J., Droxler, A.W., 2014. Climatic controls on hurricane patterns: a 1200-y near-annual record from Lighthouse Reef, Belize. Sci. Rep. 4, 1–7.
Donnelly, J.P., Hawkes, A.D., Lane, P., MacDonald, D., Shuman, B.N., Toomey, M.R., van Hengstum, P.J., Woodruff, J.D., 2015. Climate forcing of unprecedented intense-hurricane activity in the last 2000 years. Earth's Future 3, 49–65.
Donnelly, J.P., Woodruff, J.D., 2007. Intense hurricane activity over the past 5,000 years controlled by El Nino and the West African monsoon. Nature 447, 465–468.
Elsner, J., Liu, K., Kocher, B., 2000. Spatial variations in major US hurricane activity: statistics and a physical mechanism. J. Clim. 13, 2293–2305.
Elsner, J.B., Kossin, J.P., Jagger, T.H., 2008. The increasing intensity of the strongest tropical cyclones. Nature 455, 92–95.
Emile-Geay, J., Cobb, K.M., Mann, M.E., Wittenberg, A.T., 2013. Estimating central equatorial pacific SST variability over the past millennium. Part II: reconstructions and implications. J. Clim. 26, 2329–2351.
Ercolani, C., Muller, J., Collins, J., Savarese, M., Squiccimara, L., 2015. Intense Southwest Florida hurricane landfalls over the past 1000 years. Quat. Sci. Rev. 126, 17–25.
Goldenberg, S.B., Landsea, C.W., Mestas-Nunez, A.M., Gray, W.M., 2001. The recent increase in Atlantic hurricane activity: causes and implications. Science 293, 474–479.
Gray, W.M., 1984. Atlantic seasonal hurricane frequency. Part I: El Nino and 30 mb quasi-biennial oscillation influences. Mon. Weather Rev. 112, 1649–1668.
Haigh, J.D., 1996. The impact of solar variability on climate. Science 272, 981–984.
Hodges, R.E., Jagger, T.H., Elsner, J.B., 2014. The sun-hurricane connection: diagnosing the solar impacts on hurricane frequency over the North Atlantic basin using a space–time model. Nat. Hazard. 73, 1063–1084.
Huang, N.E., Wu, Z., 2008. A review on Hilbert-Huang transform: method and its applications to geophysical studies. Rev. Geophys. 46, RG2006.
Ineson, S., Scaife, A.A., Knight, J.R., Manners, J.C., Dunstone, N.J., Gray, L.J., Haigh, J. D., 2011. Solar forcing of winter climate variability in the Northern Hemisphere. Nat. Geosci. 4, 753e757.

Jagger, T.H., Niu, X., Elsner, J.B., 2002. A space-time model for seasonal hurricane prediction. Int. J. Clim. 22, 451–465.
Jahan, S., Wang, Y., Burnett, W.C., Means, G.H., Sun, F., 2021. Evaluating organic geochemical proxies for application to coastal lake sediments along the Gulf Coast of Florida for paleotempestology. Quat. Sci. Rev. 266, 107077.
Kim, H.M., Webster, P.J., Curry, J.A., 2009. Impact of shifting patterns of pacific ocean warming on North Atlantic tropical cyclones. Science 325, 77–80.
Knudsen, M., Seidenkrantz, M., Jacobsen, B.H., Kuijpers, A., 2010. Tracking the atlantic multidecadal oscillation through the last 8,000 years. Nat. Commun. 2, 178.
Knutson, T., Camargo, S.J., Chan, J., Emanuel, K., Ho, C.H., Kossin, J., Mohapatra, M., Satoh, M., Sugi, M., Walsh, K., Wu, L.G., 2020. Tropical cyclones and climate change assessment: Part II. Projected response to anthropogenic warming. Bull. Am. Meteorol. Soc. 101, E303–E322.
Kossin, J.P., Camargo, S.J., Sitkowski, M., 2010. Climate modulation of North Atlantic hurricane tracks. J. Clim. 23, 3057–3076.
Kossin, J.P., Knapp, K.R., Olander, T.L., Velden, C.S., 2020. Global increase in major tropical cyclone exceedance probability over the past four decades. Proc. Natl. Acad. Sci. U.S.A. 117, 11975–11980.
Kozar, M.E., Mann, M.E., Camargo, S.J., Kossin, J.P., Evans, J.L., 2012. Stratified statistical models of North Atlantic basin-wide and regional tropical cyclone counts. J. Geophys. Res.: Atmospheres 117, 1–13.
Lakewatch, F., 2008. A Management Plan for Walton County's Coastal Dune Lakes. University of Florida, p. 31.
Lambert, W.J., Aharon, P., Rodriguez, A.B., 2008. Catastrophic hurricane history revealed by organic geochemical proxies in coastal lake sediments: a case study of Lake Shelby, Alabama (USA). J. Paleolimnol. 39, 117–131.
Lane, P., Donnelly, J., Woodruff, J., Hawkes, A., 2011. A decadally-resolved paleohurricane record archived in the late Holocene sediments of a Florida sinkhole. Mar. Geol. 287, 14–30.
Lapointe, F., Bradley, R., Francus, P., Balascio, N., Abbott, M., Stoner, J., St-Onge, G., Coninck, A., Labarre, T., 2020. Annually resolved Atlantic sea surface temperature variability over the past 2,900 y. Proc. Natl. Acad. Sci. U.S.A. 117, 27171–27178.
Lin, N., Lane, P., Emanuel, K.A., Sullivan, R.M., Donnelly, J.P., 2014. Heightened hurricane surge risk in northwest Florida revealed from climatological-hydrodynamic modeling and paleorecord reconstruction. J. Geophys. Res.: Atmospheres 119, 8606–8623.
Mann, M., Woodruff, J., Donnelly, J., Zhang, Z., 2009a. Atlantic hurricanes and climate over the past 1500 years. Nature 460, 880–883.
Mann, M.E., Zhang, Z.H., Rutherford, S., Bradley, R.S., Hughes, M.K., Shindell, D., Ammann, C., Faluvegi, G., Ni, F.B., 2009b. Global signatures and dynamical origins of the little ice age and medieval climate anomaly. Science 326, 1256–1260.
McCloskey, T., Bianchette, T., Liu, K., 2013. Track patterns of landfalling and coastal tropical cyclones in the Atlantic basin, their relationship with the north atlantic oscillation (NAO), and the potential effect of global warming. American J. Clim. 2, 12e22.
McCloskey, T., Liu, K., 2012. A sedimentary-based history of hurricane strikes on the southern caribbean coast of Nicaragua. Quat. Res 78, 454–464.
McCloskey, T., Liu, K., 2013. A 7000-year record of paleohurricane activity from a coastal wetland in Belize. Holocene 23, 276–289.
Meyers, P.A., 1997. Organic geochemical proxies of paleoceanographic, paleolimnologic, and paleoclimatic processes. Org. Geochem. 27, 213–250.
Milliken, K., Anderson, J.B., Rodriguez, A.B., 2008. A new composite Holocene sea-level curve for the northern Gulf of Mexico. In: Anderson, J.B., Rodriguez, A.B. (Eds.), Response of Upper Gulf Coast Estuaries to Holocene Climate Change and Sea Level Rise. Geological Society of America, pp. 1–11.
Moy, C.M., Seltzer, G.O., Rodbell, D.T., Anderson, D.M., 2002. Variability of El niño/southern oscillation activity at millennial timescales during the Holocene epoch. Nature 420, 162–165.
Muller, J., Collins, J.M., Gibson, S., Paxton, L., 2017. Recent advances in the emerging field of paleotempestology. In: Collins, J.M., Walsh, K. (Eds.), Hurricanes and Climate Change. Springer, pp. 1–33.
Muller, J., Ercolani, C., Collins, J., Ellis, S., 2022. Multi-proxy characterization of storm deposits on Sanibel Island, Florida: a modern analog for paleotempestology. Geomorphology 402, 108148.
NCEI, 2021. NOAA national centers for environmental information. https://www.ncdc.noaa.gov/billions/.
Nurnberg, D., Ziegler, M., Karas, C., Tiedemann, R., Schmidt, M.W., 2008. Interacting loop current variability and Mississippi River discharge over the past 400 kyr. Earth Planet Sci. Lett. 272, 278–289.
Puri, H.S., Vernon, R.O., 1964. Summary of the Geology of Florida and a Guidebook to the Classic Exposures. Florida Geological Survey.
Reimer, P.J., Austin, W.E., Bard, E., Bayliss, A., Blackwell, P.G., Ramsey, C.B., Butzin, M., Cheng, H., Edwards, R.L., Friedrich, M., Grootes, P.M., Guilderson, T.P., Hajdas, I., Heaton, T.J., Hogg, A.G., Hughen, K.A., Kromer, B., Manning, S., Muscheler, R., Palmer, J.G., Pearson, C., van der Plicht, J., Reimer, R.W., Richards, D.A., Scott, E. M., Southon, J.R., Turney, C., Wacker, L., Adolphi, F., Buntgen, U., Capano, M., Fahrni, S.M., Fogtmann-Schulz, A., Friedrich, R., Köhler, P., Kudsk, S., Miyake, F., Olsen, J., Reinig, F., Sakamoto, M., Sookdeo, A., Talamo, S., 2020. The IntCal20 northern hemisphere radiocarbon age calibration curve (0-55 cal kBP). Radiocarbon 62, 725–757.
Rodysill, J., Donnelly, J., Sullivan, R., Lane, P., Toomey, M., Woodruff, J., Hawkes, A., MacDonald, D., d'Entremont, N., McKeon, K., Wallace, E., van Hengstum, P., 2020. Historically unprecedented Northern Gulf of Mexico hurricane activity from 650 to 1250 CE. Sci. Rep. 10, 19092.
Rustic, G.T., Koutavas, A., Marchitto, T.M., Linsley, B.K., 2015. Dynamical excitation of the tropical pacific ocean and ENSO variability by little ice age cooling. Science 350, 1537–1541.
Schmidt, W., 1984. Neogene Stratigraphy and Geologic History of the Apalachicola Embayment. Florida Geological Survey Bulletin Florida Geological Survey, Florida, p. 146. Florida.
Schmitt, D., Gischler, E., Anselmetti, F.S., Vogel, H., 2020. Caribbean cyclone activity: an annually-resolved Common Era record. Sci. Rep. 10, 1–17.
Schneider, T., Hampel, H., Mosquera, P.V., Tylmann, W., Grosjean, M., 2018. Paleo-ENSO revisited: Ecuadorian Lake Pallcacocha does not reveal a conclusive El Niño signal. Global Planet. Change 168, 54–66.
Sinclair, W.C., Stewart, J.W., 1985. Tallahassee, Florida Sinkhole Type, Development, and Distribution in Florida, Map Series No. 110. Florida Geological Survey, Tallahassee, Florida.
Steinhilber, F., Abreu, J.A., Beer, J.r., Brunner, I., Christl, M., Fischer, H., Heikkilä, U., Kubik, P.W., Mann, M., McCracken, K.G., Miller, H., Miyahara, H., Oerter, H., Wilhelms, F., 2012. 94000 years of cosmic radiation and solar activity from ice cores and tree rings. Proc. Natl. Acad. Sci. U.S.A. 109, 5967–5971.
Stuiver, M., Grootes, P.M., Braziunas, T.F., 1995. The GISP2 δ18O climate record of the past 16,500 years and the role of the sun, ocean and volcanoes. Quat. Res. 44, 341–354.
Sullivan, R.M., van Hengstum, P.J., Donnelly, J.P., Tamalavage, A.E., Winkler, T.S., Little, S.N., Mejia-Ortiz, L., Reinhardt, E.G., Meacham, S., Schumacher, C., Korty, R., 2022. Northeast yucatan hurricane activity during the maya classic and postclassic periods. Sci. Rep. 12, 20107.
Thirumalai, K., Quinn, T., Okumura, Y., Richey, J., Partin, J., Poore, R., Moreno-Chamarro, E., 2018. Pronounced centennial-scale Atlantic Ocean climate variability correlated with Western Hemisphere hydroclimate. Nat. Commun. 9, 292.
Trouet, V., Harley, G., Domínguez-Delmás, M., 2016. Shipwreck rates reveal Caribbean tropical cyclone response to past radiative forcing. Proc. Natl. Acad. Sci. U.S.A. 113, 3169–3174.
USGS, 2000. The sun and climate. USGS Fact Sheet FS-095-00. https://pubs.usgs.gov/fs/fs-0095-00/fs-0095-00.pdf.
Vinther, B.M., Buchardt, S.L., Clausen, H.B., Dahl-Jensen, D., Johnsen, S.J., Fisher, D.A., Koerner, R.M., Raynaud, D., Lipenkov, V., Andersen, K.K., Blunier, T., Rasmussen, S. O., Steffensen, J.P., Svensson, A.M., 2009. Holocene thinning of the Greenland ice sheet. Nature 461, 385–388.
Wallace, E., Coats, S., Emanuel, K., Donnelly, J., 2021a. Centennial-scale shifts in storm frequency captured in paleohurricane records from the Bahamas arise predominantly from random variability. Geophys. Res. Lett. 48, e2020GL091145.
Wallace, E., Donnelly, J., van Hengstum, P., Winkler, T., Dizon, C., LaBella, A., Lopez, I., d'Entremont, N., Sullivan, R., Woodruff, J., Hawkes, A., Maio, C., 2021b. Regional shifts in paleohurricane activity over the last 1500 years derived from blue hole sediments offshore of Middle Caicos Island. Quat. Sci. Rev. 268, 107126.
Wang, C., Lee, S.K., 2010. Is hurricane activity in one basin tied to another? EOS, Transactions, American Geophysical Union 91, 93–100.
Wang, Y., Das, O., Xu, X., Liu, J., Jahan, S., Means, G.H., Donoghue, J., Jiang, S., 2019. Implications of radiocarbon ages of organic and inorganic carbon in coastal lakes in Florida for establishing a reliable chronology for sediment-based paleoclimate reconstruction. Quat. Res. 91, 638–649.
Wu, Z., Huang, N.E., 2004. A study of the characteristics of white noise using the empirical mode decomposition method. Proc. R. Soc. Lond. Ser. A 460, 1597–1611. https://doi.org/10.1098/rspa.2003.1221.
Wu, Z., Huang, N.E., 2009. Ensemble empirical mode decomposition: a noise-assisted data analysis method. Adv. Adapt. Data Anal. 1, 1–41.